Title: Astrocytic connexin43 phosphorylation contributes to seizure susceptibility after mild Traumatic Brain Injury

Abbreviated title: Cx43 phosphorylation after TBI contributes to seizures

Authors: Carmen Muñoz-Ballester[1,#], Owen Leitzel[1], Samantha Golf[1], Chelsea M Phillips[2], Michael J Zeitz[2], Rahul Pandit[1], James W. Smyth[2,3,4], Samy Lamouille* [2,3,4], Stefanie Robel*[1,5]

1 Cell, Developmental and Integrative Biology Department, University of Alabama at Birmingham, Birmingham, 21353, AL

Currently: Department of Biological Sciences, University of Maryland Baltimore County, Catonsville, 21250, Maryland

2 Fralin Biomedical Research Institute at Virginia Tech Carilion, Roanoke, 24016, VA

3 Department of Biological Sciences, College of Science, Virginia Tech, Blacksburg, 24061, VA

4 Virginia Tech Carilion School of Medicine, Roanoke, 24016, VA

5 Department of Physical Medicine and Rehabilitation, University of Alabama at Birmingham, Birmingham, 35212, AL

* Co-corresponding authors:

Stefanie Robel, srobel@uab.edu; Samy Lamouille, lamouils@vtc.vt.edu

Conflict of interest statement:

S.L. is Co-founder and CEO of Acomhal Research Inc. The rest of the authors declare no competing financial interests.

Acknowledgments:

The authors want to acknowledge the contribution of Pratishtha Panigrani and Maame Boateng to this work, by organizing images and data. This work was supported by the National Institutes of Health grants from the National Institute of Neurological Disorders and Stroke (R21NS107941 to SR and SL; R01NS121145 to SR), and the National Heart Lung and Blood Institute (R01HL159512 to JWS). Research reported carried by CMB was supported by the National Institutes of Health Common Fund under Award Number U54CA272205. The content is solely the responsibility of the authors and does not necessarily represent the official views of the National Institutes of Health. OL was supported by the Cell and Molecular Biology Training Grant T32GM146611. RP was supported by the UAB Center for Community OutReach Development (CORD) Summer program. Research reported in this publication was supported by the UAB High Resolution Imaging Facility.

Abstract

Astrocytes play a crucial role in maintaining brain homeostasis through functional gap junctions (GJs) primarily formed by connexin43 (Cx43). These GJs facilitate electrical and metabolic coupling between astrocytes, allowing the passage of ions, glucose, and metabolites. Dysregulation of Cx43 has been implicated in various pathologies, including traumatic brain injury (TBI) and acquired epilepsy. We previously identified a subset of atypical astrocytes after mild TBI that exhibit reduced Cx43 expression and coupling and are correlated with the development of spontaneous seizures. Given that mild TBI affects millions globally and can lead to long-term complications, including post-traumatic epilepsy, understanding the molecular events post-TBI is critical for developing therapeutic strategies.

In the present study, we assessed the heterogeneity of Cx43 protein expression after mild TBI. In accordance with our previous findings, a subset of astrocytes lost Cx43 expression. As previously reported after TBI, we also found a significant increase in total Cx43 protein expression after mild TBI, predominantly in the soluble form, suggesting that while junctional Cx43 protein levels remained stable, hemichannels and cytoplasmic Cx43 were increased. We then investigated the phosphorylation of Cx43 at serine 368 after TBI, which is known to influence GJ assembly and function. Phosphorylation of Cx43 at serine 368 is elevated following TBI and $Cx43^{S368A}$ mutant mice, lacking this phosphorylation, exhibited reduced susceptibility to seizures induced by pentylenetetrazol (PTZ). These findings suggest that TBI-induced Cx43 phosphorylation enhances seizure susceptibility, while inhibiting this modification presents a potential therapeutic avenue for mitigating neuronal hyperexcitability and seizure development.

Significance statement

Connexin43 (Cx43) is the main protein of astrocyte gap junctions, mediating astrocyte coupling of astrocytes into cellular networks, but has also other non-junctional functions. Many pathologies present with altered Cx43 regulation. In this study, we studied Cx43 alterations after mild traumatic brain injury (TBI) in a mouse model. We found that while some astrocyte lost Cx43 expression, a subset of astrocytes experienced an increase in cytoplasmic and hemichannel Cx43. This increase correlated with an increase in phosphorylated Cx43 at serine 368. $Cx43^{S368A}$ mutant mice, lacking this phosphorylation, exhibited reduced susceptibility to seizures induced by pentylenetetrazol (PTZ). These findings suggest that TBI-induced Cx43 phosphorylation enhances seizure susceptibility.

Introduction

Astrocytes maintain brain homeostasis in part through functional gap junctions (GJs) comprising the protein connexin43 (Cx43). Cx43 is the primary GJ protein expressed in astrocytes and mediates coupling of astrocytes into vast cellular networks. These junctions enable electrical and metabolic coupling, allowing ions and metabolites to transfer between astrocytes. Many pathologies, including traumatic brain injury (TBI) (B. Chen et al., 2017; W. Chen et al., 2019; Wu et al., 2013; Xia et al., 2024) and acquired epilepsy (Bedner et al., 2015; Deshpande et al., 2017; Walrave et al., 2018) exhibit altered Cx43 regulation, and are often equated to GJ dysfunction. Yet, Cx43 also has non-junctional and channel-independent functions, including hemichannel communication with the extracellular milieu, cell adhesion, and intracellular signaling (reviewed in Martins-Marques et al., 2019).

We recently reported Cx43 expression and astrocyte coupling decrease in a specific subset of atypical astrocytes, which are linked to spontaneous seizures (Shandra et al., 2019). TBI affects 64 to 69 million people worldwide each year (Dewan et al., 2018). Approximately 70% of all TBI cases are mild and yet even mild TBI can lead to long-term consequences, such as impaired cognitive function, emotional regulation and sleep (Mantua et al., 2017). Mild TBI also increases the risk for developing co-morbidities including post-traumatic epilepsy (Sødal et al., 2024; Verellen & Cavazos, 2010). Currently, no clinical interventions exist to prevent these outcomes, partly due to unresolved early molecular and cellular events post-TBI.

Reduced Cx43-mediated astrocyte coupling is thought to contribute to neuronal dysfunction (Steinhäuser et al., 2012), potentially through impaired spatial potassium (K^+) buffering. When K^+ is elevated in the extracellular space, neurons depolarize, which can result in hyperexcitability. When the delicate balance of neuronal inhibition and excitation is disrupted, lack of Cx43/Cx30 is expressed in astrocytes albeit at lower levels than Cx43 and can participate in gap junction formation–appears to promote neuronal hyperexcitability. In contrast, Cx43/Cx30 may also promote and sustain neuronal hyperactivity and subsequent damage

because astrocyte coupling is needed to distribute glucose and lactate to feed neuronal activity (Deshpande et al., 2017; Khan et al., 2016).

Many studies assessing the role of astrocyte Cx43 in pathology were conducted in mice with widespread deficiency in both Cx30 and Cx43 Yet, after mild TBI, our previous study showed reduction of Cx43 only in a small subset of atypical astrocytes while Cx43 was present in most astrocytes. As most previous studies that assessed Cx43 used bulk analysis, this heterogeneity has remained unexamined in the context of TBI.

Further, Cx43 KO mice (Rouach et al., 2008) as well as gene deletion approaches or Cx43 siRNA (Ichkova et al., 2019), which target Cx43 transcripts, affect Cx43 GJ channel-dependent and independent functions. Cx43 can also remain undocked, forming hemichannels which may release small molecules, such as glutamate or ATP into the extracellular space driving pathology (Orellana et al., 2011; Retamal et al., 2006; Stout et al., 2002; Ye et al., 2003).

GJs are dynamic structures that turn-over constantly under normal conditions and therefore remodel rapidly after insult. Cx43 localization and activity are regulated by several kinases modulating phosphorylation of key residues within the Cx43 carboxy terminus. $Cx43^{S368}$ phosphorylation is mediated by protein kinase C (PKC) and has been implicated in preventing new GJs from assembling, while negatively impacting channel opening probability (Calhoun et al., 2020; Ek-Vitorin et al., 2006; Lampe et al., 2000; Sirnes et al., 2009). During acute cardiac ischemia, phosphorylation at S368 precedes ubiquitination of Cx43, leading to its degradation (Martins-Marques et al., 2015; Smyth et al., 2014). Mice harboring a serine to alanine mutation at $Cx43^{S368}$ ($Cx43^{S368A}$) to prevent phosphorylation have demonstrated protection against pathological cardiac conduction slowing during acute infection, attributed to maintenance of gap junction coupling (Gy et al., 2011; Padget et al., 2024). However, the $Cx43^{S368A}$ mutation has also been implicated in reducing hemichannel opening probability during ischemia/reperfusion indicating distinct roles for this phosphorylation event on channel function (Hirschhäuser et al.,

2021). In animal models of and patients with epilepsy and TBI, Cx43^{S368} is increased, providing correlative evidence for its importance (W. Chen et al., 2018; Greer et al., 2017). Yet, how Cx43 is regulated after TBI and whether S368 can be causally linked to seizure susceptibility has not yet been determined.

Here we first assessed the heterogeneity of Cx43 protein expression after mild TBI. As previously reported, we confirmed a subset of astrocytes had lost Cx43 protein expression (Shandra et al., 2019). Yet surprisingly, we observe an overall increase in Cx43 expression at three days after mild TBI with remarkable heterogeneity between groups of astrocytes. We determined that junctional Cx43 remains largely unchanged while the soluble fraction, which contains hemichannels and cytoplasmic Cx43, accounts for the increase in protein expression. Hemichannel activity was increased in some but not all mice. Finally, we observed Cx43 is phosphorylated at S368 after TBI, and Cx43^{S368A} mice, which lack phosphorylation at Cx43^{S368}, were less susceptible to seizures in response to PTZ kindling after mild TBI. Together, these results suggest that mild TBI induces phosphorylation of Cx43 on S368, which confers a higher seizure susceptibility, and inhibition of Cx43 phosphorylation at Ser368 may represent therapeutic potential in suppressing neuronal hyperexcitability and seizures following TBI.

Material and methods

Animals

Eight to sixteen male and female mice were used for experiments. C57Bl/6 mice were bred in-house, and breeders were purchased from The Jackson Laboratory (JAX #000664). Cx43^{S368A} mice were kindly provided by Dr. Paul Lampe at the Fred Hutchinson Cancer Research Center in (Abd-Elfattah Foda & Marmarou, 1994; Foda & Marmarou, 1994; Marmarou et al., 1994; Nichols et al., 2016; Shandra & Robel, 2020)Colonies were maintained in a standard pathogen restricted barrier animal facility in groups of 7 mice at maximum on a 12 h light/12 h dark cycle in the Fralin Biomedical Research Institute (Virginia Tech) animal facility or at the University of Alabama at Birmingham animal facility. Humidity and temperature were constant (22°C), with food and water provided ad libitum. After all procedures, mice were housed either alone or with littermates that were a part of the same experimental condition until the desired endpoint was reached.

All animal procedures were approved and conducted according to the guidelines of the Institutional Animal Care and Use Committee of Virginia Polytechnic and State University and/or the University of Alabama at Birmingham. The protocols were done in compliance with the National Institute of Health's Guide for the Care and Use of Laboratory Animals.

Weight drop model

We used an impact acceleration weight drop model, as described previously (Shandra & Robel, 2020). Briefly, mice were anesthetized using 3.5% isoflurane for five minutes. Immediately after that and while they were still unconscious, mice were administered the analgesic buprenorphine (0.05-1.00 mg/kg) placed on a foam, a metal plate was positioned over their head to create a diffuse injury, and a 100 g weight was dropped from a 50 cm height. Mice were placed over a

heat pad until consciousness was recovered. Sham mice (control) went through the same analgesics and anesthesia procedures but were not hit by the weight. For most of the experiments three injuries with 45 minutes between them were inflicted. In experiments in which Cx43^{S368A} were used, mice were only injured twice, with 45 minutes between the injuries due to an increased mortality both in sham and TBI group.

Western blot

Male and female mice were sacrificed by cervical dislocation at the time indicated in the experiment. Their brain was extracted and the cortices isolated, snap frozen in liquid nitrogen, and stored at -80ºC. Tissues were mechanically homogenized in 0.5 mL of lysis buffer (50 mM TrisHCl, 150 mM NaCl, 2% NP-40, 1% sodium deoxycholate acid (DOA), 0.1% SDS at pH 8.0, phosphatase inhibitors and protease inhibitors (Sigma-Aldrich, catalog #P8340, #P0044)), followed by sonication (3× 10 s pulse/rest 5 s, 30% amplitude) on ice. Samples were incubated on ice for 15 minutes and centrifuged for 5 minutes at 1400 x *g* at 4ºC. The pellet was discarded, and the supernatant protein concentration was analyzed using a bicinchoninic acid assay (BCA, Pierce, ThermoFisher Cat. #23225). 15 µg of protein was mixed with sample buffer (4× Laemmli sample buffer with β-mercaptoethanol) and 1:10 dithiothreitol, denatured at 95°C for 5 min, and loaded into Bio-Rad Criterion TGX precast 18-well gels. Gels were run at 80 V until dye line narrowed and then at 200 V for ~30–45 min. The Trans-blot Turbo Transfer system was used for semidry transfer at 2.5 A and 25 V for 10 min. Membranes were blocked using Azure Blocking solution for 15 minutes and were incubated overnight at 4ºC with primary antibody (**Table 1**). After washing for 15 minutes in Azure washing solution at room temperature, the membranes were incubated with secondary antibodies for 45 minutes (**Table 1**). After incubation, the membranes were washed for 15 minutes at room temperature. Images were acquired using a Chemidoc MP imaging system (Bio-Rad).

Immunohistochemistry

Mice were anesthetized using a fatal dose of ketamine (100 mg/kg) and xylazine (10 mg/kg). When the mice were unconscious, they were transcardially perfused with PBS, followed by 4% PFA. After the brains were extracted, they were post-fixed in 4% PFA overnight, transferred to PBS and coronally sliced at 50 µm thickness. Immunohistochemistry was done as described previously (George et al., 2021; Munoz-Ballester et al., 2022; Shandra et al., 2019). Briefly, 5-6 brain slices from different areas of the brain were incubated in primary (**Table 2**) overnight at 4ºC in a rocking platform. After washes in PBS, slices were incubated in secondary antibody (**Table 2**) with 4',6-diamidino-2-phenylindolefor (DAPI, 1:1000, Invitrogen) 45 minutes at room temperature in a rocking platform, washed in PBS and mounted using Aqua-Poly/Mount (Polysciences). After drying, imaging was done using a NikonA1R confocal microscope with Apo 20x air objective and Apo 40x and 60x oil immersion objectives. The size of the step used was 1 µm. We imaged cortical layers I-III throughout the entire cortex excluding the piriform cortex for all analysis. At least 3 different slices of each mouse were imaged. For each mouse, 5 images from 2-5 different slices were taken and analyzed.

Solubility assay

Snap-frozen tissue samples were weighed and added to 1% Triton X-100 buffer (50 mM Tris pH 7.4, 1% Triton X-100, 2 mM EDTA, 2 mM EGTA, 250 mM NaCl, 1 mM NaF, 0.1 mM Na_3VO_4; supplemented with Halt protease and phosphatase inhibitor cocktail, Thermo Fisher) at a final concentration of 100 mg/ml. Samples were homogenized using a bead mill and nutated for 1 h at 4°C. At this point, 10% of the lysate was removed and 4X LDS NuPAGE sample buffer (Thermo Fisher) supplemented with 400 mM DTT was added prior to sonication and

centrifugation at 10,000 x *g* for 20 min to obtain the 'total' fraction. The remaining lysate was fractionated by centrifugation for 30 min at 15,000 x *g* in pre-weighed microcentrifuge tubes. The supernatant was removed and combined with 4X LDS NuPAGE sample buffer prior to sonication and centrifugation at 10,000 x *g* for 20 min to obtain 'soluble' fraction. Pellets were weighed and suspended in 1X LDS NuPAGE sample buffer to a final concentration of 30 mg/ml. Pellets were solubilized with disruption by serial passage through an insulin syringe and sonication prior to centrifugation at 10,000 x *g* for 20 min. Protein samples were denatured by heating at 70 °C for 10 min and underwent SDS-PAGE with NuPAGE Bis-Tris 4-12% gradient gels and MES running buffer (Thermo Fisher). Proteins were transferred to LF-PVDF membranes (Bio-Rad), with membranes methanol-fixed and air-dried post-transfer. Following methanol reactivation, membranes were blocked in 5 % nonfat milk (Carnation) in TNT buffer (0.1 % Tween 20, 150 mM NaCl, 50 mM Tris pH 8.0) for 1 h at room temperature. Primary antibody incubation was conducted overnight at 4 °C using rabbit anti-Cx43 (1:4,000; Sigma-Aldrich) and mouse anti-GAPDH (1:500; Santa Cruz Biotechnology). Membranes were rinsed twice and washed 3 x 10 min in TNT buffer. Secondary antibody labeling was conducted for 1 h at room temperature using antibodies conjugated to Alexa Fluor 555 and Alexa Fluor 647 (Thermo Fisher). Following the secondary antibody incubation, membranes were washed in TNT buffer as previously described. Prior to imaging, membranes were fixed in methanol and air dried. Images were acquired using a Chemidoc MP imaging system (Bio-Rad). Western blot quantification was conducted using Bio Rad Image Lab software.

Super-resolution imaging

Super-resolution imaging was performed in Layer 2/3 of somatosensory cortex in 50µm coronal brain slices using a Nikon AX R Confocal Microscope System with NSPARC. Images were acquired with a 60x objective and 5x digital zoom. Imaging was conducted using a Galvano

scanner to capture z-stacks. The initial plane of focus was identified at the top of each tissue slice from which 1-micron thick z-stacks were taken with a step size of 0.1 microns. A total of 15 z-stacks were captured per mouse in 3 different brain sections (5 z-stacks per section). Imaging parameters were applied consistently throughout the experiment. Z-stacks were subsequently deconvolved in Nikon NIS-Elements software using blind deconvolution with 10 iterations. For analysis, the fourth plane from the top of each slice was selected.

Ethidium bromide assay

Three days after inducing TBI mice were sacrificed by cervical dislocation and their brains were rapidly removed and immersed in ice-cold cutting solution (in mM): 135 N-methyl-D-gluoconate (NMDG), 1.5 KCl, 1.5 KH_2PO_4, 23 choline bicarbonate, 25 D-glucose, 0.5 $CaCl_2$ 2.5 $MgSO_4$. Slices of 200 uM were cut using a vibratome and placed on 6 well plate with hanging cell culture inserts, one for each condition, in carbogen-bubbled artificial cerebrospinal fluid (ACSF) (in mM)125 NaCl, 3 KCl, 1.25 NaH_2PO_4, 25 $NaHCO_3$, 2 $CaCl_2$, 1.3 $MgSO_4$, 25 D-glucose at room temperature. After 10 minutes in ACSF as recovery time, a different treatment was added to each well and incubated for 15 minutes. The treatments were: water, DMSO, 200 µM carbenoxolone disodium salt (CBX) (Sigma-Aldrich), 10 µM spironolactone (Sigma-Aldrich) and 2 µM the hemichannel inhibitor peptide TAT-Gap19 (YGRKKRRQRRRKQIEIKKFK, synthetized by Genscript). Slices in water were used as control for CBX and TAT Gap19 slices. DMSO slices were used as control for the spironolactone treatment. Following the treatment incubation, 4 µM ethidium bromide (EtBr) was added to the well and incubated for 15 minutes, followed by a 10-minute wash in ACSF. Slices were fixed in 4% PFA for 20 minutes. After that, immunohistochemistry against s100b and imaging was initiated as described in the immunohistochemistry section. No DAPI was used in this experiment.

Seizure susceptibility assay using sub-convulsive dosing of Pentylenetetrazole

To determine seizure susceptibility, C57Bl/6 and Cx43^{S368A} TBI, Sham (all procedures as in TBI mice including administration of isoflurane and buprenorphine except for the weight drop) or naïve mice (no isoflurane or buprenorphine) were injected with sub-convulsive doses of Pentylenetetrazole (PTZ) on alternating days, starting on day 3 following TBI/Sham. Naïve C57Bl/6 and Cx43^{S368A} mice were injected 8–11 times, TBI/Sham C57Bl/6 and Cx43^{S368A} mice were injected 11 times. PTZ was made freshly for each session at with 3.5 mg/mL in saline followed by intraperitoneal administration of 10 µL/g body weight (35 µg/g body weight). Following PTZ injection, mice were observed for 30 min before mice were returned to their home cage. Behavioral abnormalities indicating seizures were scored according to a modified Racine scale (Dhir, 2012). In short, a score of 0 indicated no behavioral abnormalities, freezing behavior or laying down was scored as 1, shaking and twitching 2, forelimb clonus, lordotic posture and tail erection were scored 3, rearing and falling were scored 4 and generalized, tonic-clonic seizures, wild jumping, loss of postural tone sometimes resulting in death were scored as 5. The time to onset of generalized, tonic-clonic seizures was recorded. One mouse died 5 seconds after the injection and was excluded from the study given that mortality was likely due to an inappropriate injection site.

Data analysis

Western Blot quantification

Western blot images were imported as a third-party image and analyzed using Image Studio software (Li-Cor) (**Fig. 1, 4**) or ImageLab (BioRad) (**Fig. 2**). Cx43 or pCx43^{S368} bands were identified using the automatic *Add rectangle* function of Studio Image, and rectangular volume analysis in ImageLab. For the solubility assay, insoluble (junctional) fraction values are

expressed relative to soluble (non-junctional) values from the same samples. The background was calculated based on the median intensity at the top and bottom area surrounding the band (3 pixels). The normalized value of the signal based on the background that was provided by the program was used as the intensity value. GAPDH was used as an internal control and the intensity of its signal was calculated in the same way. In each experiment, the average of the ratio Cx43/GAPDH of sham mice was considered 100% and used to normalize all values.

Cx43 fluorescence intensity quantification

The mean, standard deviation, and kurtosis of Cx43 signal was calculated per image using the *Measurement* function of Fiji is Just Image J (FIJI). The value of each slice was averaged per mouse. The average of sham mice was considered 100% and each value was normalized based on that. Images containing the meninges were excluded from the analysis, since meningeal fibroblasts express high levels of Cx43 and biased the result.

Cx43 super-resolution measurements of plaque size and density

General Analysis 3 imaging processing and measuring module in the Nikon imaging software, NIS-Elements, was used to threshold super resolution images to eliminate background signal before binarization to isolate Cx43 signal. NIS-Element's General Analysis 3's ObjectCount, ObjectArea, and MeasuredArea functions were used to measure plaque number, plaque size, and image area, respectively. Average plaque size was determined by the sum of all plaque areas divided by the total number of plaques per mouse. Average density was determined by the total number of plaques divided by the total area imaged per mouse.

EtBr fluorescence intensity analysis

For each image, the soma of five astrocytes were blindly identified using s100b staining and delimited using the *Oval selection* feature of ImageJ. After that, the EtBr mean fluorescence intensity within that circle was calculated using the *Measurement* function of FIJI. The mean

fluorescence intensity of an oval selection of the tissue with no signal was used as background and subtracted from the mean fluorescence intensity values of that slice. Each value was averaged per slice and each slice was averaged per mouse. For the comparison between sham and 3 dpi mice, the average fluorescence intensity of sham mice was considered 100% and each mouse value was normalized accordingly. For the comparison between control and treatment with inhibitors within 3 dpi mice, the average fluorescence intensity of the control treatment was considered 100% and all the values were normalized based on this value. In one batch of experiments, CBX was expired, no inhibition was observed in any sample, and those values were excluded from the analysis.

Statistical analysis

Statistics were performed and graphed using GraphPad Prism 9 or 10 (GraphPad Software). Data were tested for normality using the Kolmogorov–Smirnov (KS) normality test. Before running ANOVA tests, homoscedasticity was tested using the Levene test. If the data did not meet the conditions of applicability for parametric tests, non-parametric tests were used. Statistical tests were chosen accordingly and are specified for each experiment in the results section. In each dataset, the outlier test ROUT at Q 1% was run and values identified as outliers were excluded from the analysis. For this reason, even when normalized some control groups are not at 100% of value. Two-tailed statistical tests were used unless the prediction was unidirectional. In this case, one-tailed tests were used. Post-hoc analysis was used when more than two groups. The specific test that was used was described in each experiment. All data statistics were run after averaging per mouse, data points in scatterplots represent individual mice and means were displayed as bar graphs with standard error of the mean. Exact p-values are reported within the results section and figures. While both sexes were used in the study, the

study was not powered to assess sex differences and data from mice of both sexes were combined.

Results

Mild TBI induces heterogeneous changes in astrocytic Cx43 levels throughout the cortical gray matter

To determine temporal and spatial changes in Cx43 protein levels changed after mild TBI, mice were subjected to weight drop injury. As previously described, this injury paradigm induces mild, diffuse brain injury across both hemispheres in the absence of focal lesions or astrocyte border/scar-formation (Abd-Elfattah Foda & Marmarou, 1994; Marmarou et al., 1994; Nichols et al., 2016; Shandra et al., 2019). Cortical Cx43 protein levels detected by western blot (WB) did not change 4 hpi (4hpi mean = 117.5±27.70) when compared to sham mice (Sham mean = 91.86±3.622; Krauskal-Wallis multiple comparisons test Sham vs 4hpi p-value = 0.9966). However, a significant increase in Cx43 protein was observed 3 dpi (3 dpi mean = 160.7±23.82; Krauskal-Wallis multiple comparisons test Sham vs 3 dpi p-value=0.0365) (**Fig. 1A and 1B**). When immunohistochemistry against Cx43 was performed in 3 dpi TBI mice, we observed that the Cx43 expression pattern was heterogeneous: while some areas had a significant decrease in Cx43, other areas had increased levels of Cx43 with a higher density of the signal (**Fig. 1C and D**). The surface plot in which the height of a certain point/pixel is proportional to the intensity of said pixel (**Fig. 1E**) also reflected a higher heterogeneity in the fluorescence intensity 3 dpi compared to the sham. However, when we analyzed mean fluorescence intensity levels, we did not find significant differences in the intensity (Sham mean = 99.30±9.866, n = 6; 3 dpi mean = 147.4±27.24, n = 7; unpaired two-tailed t-test p-value = 0.1484) (**Fig. 1F**) indicating that Cx43 increase observed by WB could not be detected with this methodology. We found that the variability of the samples measured as standard deviation was higher in 3 dpi compared to sham mice (Sham mean = 99.17±9.687, n = 6; 3 dpi mean = 69.83±22.59, n = 8; unpaired two-tailed t-test, p-value = 0.0217) (**Fig. 1G**) pointing to a regional heterogenous response. We also analyzed the sharpness of the peak of the fluorescence intensity data by analyzing the kurtosis

as readout for the extent to which a distribution contains outliers and found no differences between sham and 3 dpi mice (Sham mean = 99.28±13.94, n = 6; 3 dpi mean = 69.83±9.453, n = 8; unpaired two-tailed t-test p-value = 0.0946) (**Fig. 1H**). We concluded that mild TBI induces a heterogenous astrocyte response, in which Cx43 is locally regulated, being downregulated in a subset of astrocytes and increased in a different subset, without extreme values that modify the distribution of the population. This is in alignment with previous studies of astrocytes in this model in which astrocytes vary in their local responses.

Mild TBI leaves mean Cx43 gap junction density unaffected while soluble Cx43 increases

To determine if the overall increase in Cx43 is reflected in an increase in Cx43 GJ, we took advantage of the fact that Cx43 GJ cluster in large insoluble structures: junctional plaques. We performed a fractionation assay based on Cx43 solubility and analyzed the fractions using western blot. GJ plaques are enriched in the triton X-100 insoluble fraction while cytoplasmic Cx43 and uncoupled Cx43 hemichannels are contained within the soluble fraction. While no change was observed in the amount of Cx43 within the insoluble fraction (GJ) (Sham mean = 100±8.601, n = 6; 3 dpi mean = 80.91±10.11, n=9; unpaired two-tail t-test p-value = 0.2052) (**Fig. 2 A,B**), Cx43 levels in the soluble fraction (non-junctional Cx43) increased at 3 dpi (Sham mean = 100±15.81, n=6; 3 dpi mean = 152.5±14.30, n=9; unpaired two-tail t-test p-value = 0.0316) (**Fig. 2A,C**). Accordingly, the ratio of soluble to insoluble Cx43 was increased (Sham mean = 0.4744±0.07403, n=6; 3 dpi mean = 1.056±0.1729, n=9; unpaired two-tail t-test p-value = 0.0215) (**Fig. 2D)**.

We next used super-resolution imaging microscopy to determine whether the Cx43 plaques changed in density or size. In super-resolution images, junctional plaques appear as brighter discrete puncta, while non-junctional Cx43 is visible as diffuse staining. After processing the

image to isolate junctional plaques, no difference in plaque density (Sham mean = 0.4951 plaque /μm^2 ±0.02272 , n = 3; 3 dpi mean = 0.4167 plaque /μm^2 ±0.05862, n=4; unpaired two-tail t-test, p-value = 0.3255) or plaque size was found between sham and 3 dpi mice (Sham mean = 0.06139 μm^2 ±0.00456, n=3; 3 dpi mean = 0.05226 μm^2 ±0.005454; unpaired two-tail t-test p-value = 0.2777) **(Fig. 2 E–H**), suggesting that GJ turnover is not affected by TBI at 3 dpi. These results indicate that the Cx43 increase after mild TBI does not lead to increased GJ formation but instead in an increase in non-junctional Cx43.

Mild TBI may cause an increase in hemichannel activity

To assess whether the increase in Cx43 expression was due to an increase in Cx43-dependent hemichannels, we used an ethidium bromide (EtBr) uptake assay in acute slices from sham and TBI 3 dpi mice. EtBr can pass through open Cx43 hemichannels or pannexin channels on the cell surface to bind DNA, where subsequent fluorescence can be detected (Johnson et al., 2016). The fluorescence observed within the cell is proportional to the activity of the channel by which it enters. Because EtBr fluoresces in the far-red channel, Cx43 hemichannel activity of a cell can be inferred based on the fluorescence intensity of its nucleus. We quantified the EtBr fluorescence intensity of astrocytic nuclei in acute slices from Sham and 3 dpi mice and found that s100-positive astrocytes had increased EtBr fluorescence intensity 3 dpi compared to sham mice (**Fig. 3 A, B**) (Sham Mean = 100.0±2.036, n= 4; 3 dpi Mean = 185.8±14.91, n=6, one-tailed unpaired t-test p-value = 0.0009).

To determine if the increase of the EtBr signal was specific to hemichannels, we first used carbenoxolone (CBX), a broader GJ/hemichannel/pannexin blocker (Sagar & Larson, 2006). As predicted, EtBr uptake was significantly reduced in acute brain slices 3 dpi mice when compared to sham (Sham mean = 90.97 ± 38.22, n=5; mean CBX = 50.00 ± 17.45; paired one-

tail test p-value = 0.0417) **(Fig. 3 C, D**). We next assessed more specific inhibitors to determine if EtBr uptake is dependent on pannexins or Cx43 hemichannels. The pannexin blocker spironolactone (10 µM) did not reduce astrocytic EtBr (Control mean = 100.0 ± 33.80, n=6; spironolactone mean = 123.7 ± 24.93, n=6; paired one-tail test p-value = 0.1678) (**Suppl Fig. 1**) Thus, pannexin channels are not responsible for EtBr uptake into astrocytes after mild TBI. We next used the Cx43 hemichannel-specific inhibitor TAT-Gap19. EtBr uptake detected in TBI mice was decreased by 20% when TAT-Gap19 was used although this difference did not reach significance threshold (**Fig. 3 E, F**) (Sham mean = 100 ± 27.34, n=8; TAT Gap19 mean = 81.74 ± 28.18, n=8; paired one-tail t-test analysis, p=0.0901). However, while two mice had an increase or a change in EtBr uptake after TAG-Gap19 treatment (shown in red), the other six mice showed a significant reduction in EtBr uptake after blocking Cx43 hemichannel function. This may reflect heterogeneity in Cx43 regulation after mild TBI or technical variability in the diffusion of TAT-Gap19. In conclusion, EtBr uptake is increased in cortical astrocytes 3 days after mild TBI. Cx43 hemichannel contribution to this uptake occurred in two thirds of the mice while the other third responded differently, possibly indicating molecular mechanisms underlying the well-known heterogeneity in TBI outcomes from patient to patient, if not due to variable efficacy of TAT-Gap19.

Cx43 phosphorylation at serine 368 impacts seizure susceptibility

Phosphorylation at Cx43 Serine368 (pSer368) is well described in regulation of Cx43's dynamics and GJ formation, function and stability (Calhoun et al., 2020; Ek-Vitorin et al., 2006; Lampe et al., 2000; Sirnes et al., 2009). To determine if this post-translational modification was associated with the Cx43 alterations we described above in mild TBI, we assessed the levels of pSer368 by western blot and found an increase at 3 dpi (Sham mean = 100.0±23.48, n=6; 3 dpi mean = 189.0 ±23.01, n=5; two-tailed t-test p-value = 0.0253) (**Fig. 4 A,B**).

We next used mice harboring a serine-to-alanine substitution within the Cx43 368 phosphorylation site, which prevents phosphorylation of Cx43 ($Cx43^{S368A}$). $Cx43^{S368A}$ mice have significantly lower signal in WB (C57Bl/6 mean = 100.0±6.766, $Cx43^{S368A}$ mean = 5.881±1.341) (**Fig. 4C**).

We then asked whether phosphorylation at this site impacts seizure susceptibility in the context of TBI. We assessed seizure threshold by injecting subconvulsive doses of the GABA A receptor antagonist pentylenetetrazol (PTZ) on alternate days for 2-3 weeks starting 3 dpi. At this dosage, PTZ has a cumulative effect that over time increases the likelihood that a mouse seizes after injection. First, we compared uninjured, naïve C57Bl/6 and $Cx43^{S368A}$ mice (also on C57Bl/6 background). We assessed behavioral abnormalities and seizure severity using Racine scale scores 1 through 5 as described in the methods. Surprisingly, some C57Bl/6 mice already had Racine scale 5 tonic-clonic seizures after the first injection, while $Cx43^{S368A}$ mice had Racine scale 5 tonic-clonic seizures only after four PTZ injections. After six injections 50% of the C57Bl/6 mice had Racine scale 5 seizures while only 15% of the $Cx43^{S368A}$ mice did (**Fig. 4E, Suppl. Table 1**).

Next, we assessed seizure susceptibility in the context of mild TBI. As expected, TBI lowered the seizure threshold (**Fig. 4F**) resulting in 60% of C57Bl/6 mice with TBI having Racine scale 5 seizures after the third injection, while only 15% of C57Bl/6 Sham mice did at this point. It took six injections for 54% of C57Bl/6 Sham mice to present with Racine scale 5 seizures. C57Bl/6 TBI mice also had overall higher Racine scores than shams across all time points (**Fig. 4G, H**). In contrast, $Cx43^{S368A}$ mice were remarkably protected from the development of seizures compared to C57BL/6 after TBI when assessing the percentage of mice with Racine scale 5 seizures (**Fig. 4F**) or Racine scores (**Fig. 4G**). It took 8 injections for 60% of $Cx43^{S368A}$ TBI mice to display Racine scale 5 seizures. After 10 injections, all C57Bl/6 mice had tonic-clonic seizures, while only 60% of $Cx43^{S368A}$ did by the end of the experiment after 11 PTZ injections.

In summary, preventing Cx43 phosphorylation at S368 conferred protection from the development of PTZ-induced seizures in the context of mild TBI.

Gap junction plaque density is reduced in Cx43^{S368A} mice

To determine the mechanism by which a lack of phosphorylation confers protection from seizure susceptibility, we used super-resolution imaging microscopy to assess Cx43 plaque density and size in Cx43^{S368A} mice compared to C57Bl/6 controls (**Fig. 5A**) as assessed with panCx43 immunohistochemistry. These findings are consistent when using the Cx43 staining protocol performed in previous experiments (**Suppl Fig. 2**).

We observed a significant reduction in plaque density between uninjured Cx43^{S368A} and C57Bl/6 mice (Cx43^{S368A} sham mean = 0.09919 μm^2 ±0.02115, n = 3; mean C57Bl/6 sham = 0.3277 μm^2 ±0.05569, n = 3; Tukey's multiple comparisons test p-value = 0.0145) (**Fig. 5B**) but no difference in plaque size (Cx43^{S368A} sham mean = 0.05475 μm^2 ±0.002589, n = 3; C57Bl/6 sham mean = 0.06860 μm^2 ±0.097370, n = 3; Tukey's multiple comparisons test p-value = 0.4553) (**Fig. 5C**).

When comparing Cx43^{S368A} mice with and without mild TBI, we found no difference in plaque density (Cx43^{S368A} sham mean = 0.09919 plaque /μm^2 ±0.02115, n = 3; Cx43^{S368A} 3 dpi mean = 0.1302 plaque /μm^2 ±0.03416, n=3; Tukey's multiple comparisons test p-value = 0.9419) (**Fig. 5B**) or plaque size (Cx43^{S368A} sham mean = 0.05475 μm^2 ±0.002589, n=3; Cx43^{S368A} 3 dpi mean = 0.06407 μm^2 ±0.003897, n=4; Tukey's multiple comparisons test p-value = 0.7312) (**Fig. 5C**). These results demonstrate reduced gap junction densities in mice that are unable to phosphorylate S368. Although future studies need to address whether astrocytes are coupled in Cx43^{S368A} mice (i.e. if more or less GJ are open), this data suggests that a lack of phosphorylation at S368 confers protection from the development of hyperexcitability and seizures and may be a potential therapeutic target.

Discussion

Despite substantial literature reporting altered Cx43 regulation in brain pathology, there is still limited knowledge regarding the role of Cx43 and/or gap junction regulation in TBI. In many studies the expression of Cx43 mRNA or protein is interpreted as equivalent to gap junctional coupling (Deshpande et al., 2017; Garbelli et al., 2011) without consideration of the non-junctional roles of Cx43. Yet, Cx43 hemichannels, detected within the non-junctional and soluble fraction of Cx43, have been demonstrated to participate in hyperexcitability and excitotoxicity (Almad et al., 2016, 2022; Guo et al., 2022; Rovegno et al., 2015) Furthermore, how local and spatially limited dysfunction of Cx43 contributes to the progression of brain pathology had not yet been addressed. In this study, we expanded our analysis of Cx43 expression and function following mild TBI. We found that Cx43 is upregulated at the protein level, yet Cx43 expression is highly heterogeneous from astrocyte to astrocyte within the cortical gray matter. We find increased levels of Cx43 protein represent increased Cx43 hemichannel and cytoplasmic pools of Cx43, while GJ density and size are largely unchanged. Inhibiting the phosphorylation of a key regulatory site of Cx43, S368, which maintains GJ opening while reducing hemichannel opening probability, limited the seizure susceptibility of mice in both, the presence and absence of mild TBI. Future studies are needed to determine whether this is due to the overall reduction of GJ in $Cx43^{S368A}$ mice, a reduction in hemichannel opening, or changes in GJ opening/function.

Heterogeneous response of Cx43 to mild TBI within and between mice

One clear finding of the study is the high variability of Cx43 protein expression changes across the cortical gray matter within one individual, as well as between individuals. While we observed an increase in the expression of Cx43 3 days after mild TBI, the immunohistochemistry staining revealed a heterogenous expression pattern of the protein: some cortical areas had elevated Cx43, but others had a decrease or absence of it. These results might be caused by changes in the microenvironment that lead to a differential regulation of Cx43 from astrocyte to astrocyte. Previous studies in our laboratory showed that blood-brain barrier leakage induced an atypical astrocyte response characterized by significant reduction in astrocyte proteins including Cx43 that was not observed in other areas (George et al., 2021; Shandra et al., 2019). Whether areas in which Cx43 is increased to compensate Cx43 loss in other areas or whether factors upstream of Cx43 phosphorylation are responsible for the increase in Cx43 protein needs to be explored in the future. To our knowledge, such heterogenous expression of Cx43 has not been described in the brain previously and thus, investigating how this distinct local regulation affects the maintenance of brain function needs to be studied. Furthermore, these results demonstrate the need for reassessing the interpretation of previous studies that evaluate Cx43 levels exclusively by western blot. Previously, global decrease of Cx43 has been proposed as a potential therapeutic approach to ameliorate TBI outcomes (Ichkova et al., 2019). Yet, the cellular mechanism by which Cx43 contributes to seizure susceptibility and brain pathology (increase of hemichannels, closing or loss of gap junctions, or other functions of cytoplasmic Cx43) remains to be resolved.

We also found that the Cx43 global response varies between animals. Experiments that analyzed Cx43 expression levels, localization, or function all presented with high variability between individuals. Whether this variability is due to variability of the injury itself or whether it is due to other factors regulating Cx43 is not yet clear.

Cx43 increase after mild TBI is attributed to the non-junctional functions of Cx43

The role of Cx43 in forming gap junctions in the brain and other organs, has led the field to correlate an increase in Cx43 protein expression with an increase in GJ. Yet, Cx43 has other functions that are unrelated to GJ coupling of astrocytes. In this study, we differentiated between Cx43 GJ and non-junctional Cx43 using fractionation of Cx43 protein based upon solubility. We also used super-resolution imaging to identify Cx43 plaques, which are structures encompassing arrays of GJ channels, (McCutcheon 2020), and their size. Gap junctions are surprisingly dynamic structures, and alterations to plaque size occur rapidly in other systems during stress due, in part, to altered Cx43 phosphorylation (Smyth et al., 2014). Our experiments revealed that junctional Cx43 did not change in size or density, but an increase in non-junctional Cx43 was detected after mild TBI. Together with biochemical fractionation data confirming increased ‘soluble’ Cx43, we conclude that mild TBI induces increased levels of hemichannels and cytoplasmic Cx43.

There are conflicting reports regarding the relevance of hemichannels in pathology (Nielsen et al., 2017). While some reports assign important roles to astrocytic Cx43 hemichannels, others question their physiological relevance. Despite such disagreement within the field, recent work has shown that Cx43 hemichannels contribute to increased excitotoxicity and pathology in amyotrophic lateral sclerosis (ALS) (Almad et al., 2022) and temporal lobe epilepsy (Guo et al., 2022). But we are just starting to understand the participation of Cx43 hemichannels in other disorders.

In our study, we used an EtBr uptake assay to determine if the increase in soluble Cx43 was correlated with an increase in hemichannel function. Mild TBI increased EtBr uptake and this uptake was not pannexin-dependent as the pannexin 1 inhibitor spironolactone did not interfere with EtBr uptake in all mice. Using a Cx43-specific hemichannel inhibitor, EtBr uptake was reduced in 6 of 8 mice. This is in alignment with the above-discussed animal-to-animal

variability that we observed across many outcome measures. Yet, we cannot exclude the possibility that cell membranes are damaged or that other transporters like calcium homeostasis modulator (CALHM) (Gaete et al., 2020) contribute to EtBr uptake post TBI. Cell membrane disruption after traumatic brain injury may occur in neurons (Hernandez et al., 2019), which take up dyes such as 10 kDa dextran and cadaverine. In our hands, very few astrocytes take up cadaverine in areas where neurons are prominently labeled (George et al., 2021). Yet, we cannot be fully excluded that membrane disruption may contribute to ethidium bromide uptake. Furthermore, the efficiency of the TAT-Gap19 peptide in diffusing through the 300 µm acute brain slices and in blocking hemichannel function is challenging to measure and might have contributed to the heterogeneity of our results. Finally, whether increasedCx43 hemichannel activity results in a release of excitotoxic compounds as reported in other disorders need to be explored in the specific context of mild TBI. In conclusion, the increase in soluble Cx43 may result in increased hemichannel function after TBI although this possibility needs to be confirmed once more effective assays are available to univocally demonstrate their presence and activity.

Cx43^{S368} phosphorylation contributes to seizure susceptibility after mild TBI

Cx43 regulation and location is tightly regulated by post-translational modifications. One of the key regulatory sites within the Cx43 C-terminus is serine 368, which upon phosphorylation via PKC effects GJ channel closure and precedes internalization following additional phosphorylation events and ubiquitination (Calhoun et al., 2020; Ek-Vitorin et al., 2006; Lampe et al., 2000; Sirnes et al., 2009)Distinct effects of phosphorylation on GJ vs hemichannel regulation have been reported however, highlighting the importance of isolating Cx43 functions in interpretation of such findings (Hirschhäuser et al., 2021). Previous studies had shown an increase in phosphorylated Cx43^{S368} in different models of TBI. In a study using lateral fluid

percussion model the authors found an increase in pCx43^{S368} in hippocampus, which they correlated to an increase in the hemichannel-released exosomes identified by labeling with CD81 and CD63 (W. Chen et al., 2018). Yet, the authors did not assess changes in phosphorylated Cx43^{S368} in the cortex. Another study using controlled cortical impact TBI found an increase in Cx43 expression but did not find any difference in pCx43^{S368} in the subventricular zone or the hippocampus (Greer et al., 2017). Finally, a study of surgical tissue from patients with TBI of different severity showed that cortical tissue from TBI patients had increased levels of pCx43^{S368} which positively correlated with injury severity and long-term consequences of TBI, including post-traumatic epilepsy (B. Chen et al., 2017). Human and experimental temporal lobe epilepsy samples also showed an increase in pCx43^{S368} (Deshpande et al., 2017). This correlative data is in alignment with our findings after mild TBI where we found an increase in pCx43^{Ser368} in the cortex early after mild TBI (1 dpi), which was sustained for a week. Collectively, this points to an important role of pCx43^{S368} in the regulation of Cx43 in CNS pathology.

To establish whether pCx43^{Ser368} is causally related to seizure susceptibility after mild TBI, we used mice with a serine to alanine substitution at S368, which interferes with phosphorylation of Cx43 at this residue. This conferred substantial protection from the development of seizures in both injured and uninjured Cx43^{S368A} mice after subthreshold PTZ injections. While control mice that incurred a mild TBI has a significantly lower seizure threshold than uninjured mice, this increase in seizure susceptibility disappeared when Cx43^{S368} remained unphosphorylated demonstrating a key role for Cx43^{S368} in mediating pathological changes after TBI. Whether these changes are due to differences in gap junction function or attributable to other Cx43 functions, including hemichannels, needs to be resolved in future studies.

Interestingly, gap junction densities are significantly lower even in uninjured Cx43^{S368A} mice demonstrating that Cx43^{S368} does regulate GJ. Given that it has been suggested that GJ “feed”

neuronal hyperexcitability in the context of pathology, reduced gap junction densities in and of itself may be protective. However, the presence of a gap junction plaque does not reveal information about GJ conductivity. While cardiac data suggest that gap junctions in Cx43^{S368A} mice should be open at a higher probability while hemichannels should more likely be closed, this needs to be tested in future studies.

In conclusion, this study significantly advances our understanding of Cx43 response to mild TBI, going beyond Cx43 expression. The implications for hyperexcitability, potential therapeutic interventions, and the intricate post-translational modifications add layers of complexity to the ongoing discourse on Cx43 in the context of neurological injuries. While recognizing the limitations, these findings provide a crucial steppingstone for future research aiming to unravel the precise mechanisms underlying Cx43 dynamics and its broader implications for brain function post-injury.

References

Abd-Elfattah Foda, M. A., & Marmarou, A. (1994). A new model of diffuse brain injury in rats. Part II: Morphological characterization. *Journal of Neurosurgery*, *80*(2), 301–313. https://doi.org/10.3171/JNS.1994.80.2.0301

Almad, A. A., Doreswamy, A., Gross, S. K., Richard, J. P., Huo, Y., Haughey, N., & Maragakis, N. J. (2016). Connexin 43 in astrocytes contributes to motor neuron toxicity in amyotrophic lateral sclerosis. *GLIA*, *64*(7), 1154–1169. https://doi.org/10.1002/glia.22989

Almad, A. A., Taga, A., Joseph, J., Gross, S. K., Welsh, C., Patankar, A., Richard, J.-P., Rust, K., Pokharel, A., Plott, C., Lillo, M., Dastgheyb, R., Eggan, K., Haughey, N., Contreras, J. E., & Maragakis, N. J. (2022). Cx43 hemichannels contribute to astrocyte-mediated toxicity in sporadic and familial ALS. *Proceedings of the National Academy of Sciences of the United States of America*, *119*(13), e2107391119. https://doi.org/10.1073/pnas.2107391119

Bedner, P., Dupper, A., Hüttmann, K., Müller, J., Herde, M. K., Dublin, P., Deshpande, T., Schramm, J., Häussler, U., Haas, C. A., Henneberger, C., Theis, M., & Steinhäuser, C. (2015). Astrocyte uncoupling as a cause of human temporal lobe epilepsy. *Brain*, *138*(5), 1208–1222. https://doi.org/10.1093/brain/aww067

Calhoun, P. J., Phan, A. V., Taylor, J. D., James, C. C., Padget, R. L., Zeitz, M. J., & Smyth, J. W. (2020). Adenovirus targets transcriptional and posttranslational mechanisms to limit gap junction function. *The FASEB Journal*, *34*(7), 9694–9712. https://doi.org/10.1096/fj.202000667R

Chen, B., Sun, L., Wu, X., & Ma, J. (2017). Correlation between connexin and traumatic brain injury in patients. *Brain and Behavior*, *7*(9), e00770. https://doi.org/10.1002/brb3.770

Chen, W., Guo, Y., Yang, W., Chen, L., Ren, D., Wu, C., He, B., Zheng, P., & Tong, W. (2018). Phosphorylation of connexin 43 induced by traumatic brain injury promotes exosome

release. *Journal of Neurophysiology*, *119*(1), 305–311. https://doi.org/10.1152/jn.00654.2017

Chen, W., Zhao, L., Zhang, J., Wang, B., Xu, G., Lin, C., & Liu, N. (2019). Elevated expression of miR-302 cluster improves traumatic brain injury by inhibiting phosphorylation of connexin43 via ERK signaling. *Journal of Chemical Neuroanatomy*, *99*, 1–8. https://doi.org/10.1016/j.jchemneu.2019.05.003

Chever, O., Dossi, E., Pannasch, U., Derangeon, M., & Rouach, N. (2016). Astroglial networks promote neuronal coordination. *Sci Signal*, *9*(410), ra6. https://doi.org/10.1126/scisignal.aad3066

Clasadonte, J., Scemes, E., Wang, Z., Boison, D., & Haydon, P. G. (2017). Connexin 43-Mediated Astroglial Metabolic Networks Contribute to the Regulation of the Sleep-Wake Cycle. *Neuron*, *95*(6), 1365-1380.e5. https://doi.org/10.1016/j.neuron.2017.08.022

Deshpande, T., Li, T., Herde, M. K., Becker, A., Vatter, H., Schwarz, M. K., Henneberger, C., Steinhäuser, C., & Bedner, P. (2017). Subcellular reorganization and altered phosphorylation of the astrocytic gap junction protein connexin43 in human and experimental temporal lobe epilepsy. *GLIA*, *65*(11), 1809–1820. https://doi.org/10.1002/glia.23196

Dewan, M. C., Rattani, A., Gupta, S., Baticulon, R. E., Hung, Y. C., Punchak, M., Agrawal, A., Adeleye, A. O., Shrime, M. G., Rubiano, A. M., Rosenfeld, J. V., & Park, K. B. (2018). Estimating the global incidence of traumatic brain injury. *Journal of Neurosurgery*, *130*(4), 1080–1097. https://doi.org/10.3171/2017.10.JNS17352

Dhir, A. (2012). Pentylenetetrazol (PTZ) Kindling Model of Epilepsy. *Current Protocols in Neuroscience*, *58*(1), 9.37.1-9.37.12. https://doi.org/10.1002/0471142301.ns0937s58

Ek-Vitorin, J. F., King, T. J., Heyman, N. S., Lampe, P. D., & Burt, J. M. (2006). Selectivity of Cx43 channels is regulated through PKC-dependent phosphorylation. *Circulation Research*, *98*(12), 1498. https://doi.org/10.1161/01.RES.0000227572.45891.2c

Foda, M. A., & Marmarou, A. (1994). A new model of diffuse brain injury in rats. Part II: Morphological characterization. *Journal of Neurosurgery*, *80*(2), 301–313. https://doi.org/10.3171/jns.1994.80.2.0301

Gaete, P. S., Lillo, M. A., López, W., Liu, Y., Jiang, W., Luo, Y., Harris, A. L., & Contreras, J. E. (2020). A novel voltage-clamp/dye uptake assay reveals saturable transport of molecules through CALHM1 and connexin channels. *Journal of General Physiology*, *152*(11), e202012607. https://doi.org/10.1085/jgp.202012607

Gajardo-Gómez, R., Labra, V. C., Maturana, C. J., Shoji, K. F., Santibañez, C. A., Sáez, J. C., Giaume, C., & Orellana, J. A. (2017). Cannabinoids prevent the amyloid β-induced activation of astroglial hemichannels: A neuroprotective mechanism. *Glia*, *65*(1), 122–137. https://doi.org/10.1002/glia.23080

Garbelli, R., Frassoni, C., Condorelli, D. F., Trovato Salinaro, A., Musso, N., Medici, V., Tassi, L., Bentivoglio, M., & Spreafico, R. (2011). Expression of connexin 43 in the human epileptic and drug-resistant cerebral cortex. *Neurology*, *76*(10), 895–902. https://doi.org/10.1212/WNL.0b013e31820f2da6

George, K. K., Heithoff, B. P., Shandra, O., & Robel, S. (2021). Mild traumatic brain injury/ concussion initiates an atypical astrocyte response caused by blood-brain barrier dysfunction. *Journal of Neurotrauma*. https://doi.org/10.1089/NEU.2021.0204

Greer, K., Chen, J., Brickler, T., Gourdie, R., & Theus, M. H. (2017). Modulation of gap junction-associated Cx43 in neural stem/progenitor cells following traumatic brain injury. *Brain Research Bulletin*, *134*, 38–46. https://doi.org/10.1016/j.brainresbull.2017.06.016

Guo, A., Zhang, H., Li, H., Chiu, A., García-Rodríguez, C., Lagos, C. F., Sáez, J. C., & Lau, C. G. (2022). Inhibition of connexin hemichannels alleviates neuroinflammation and hyperexcitability in temporal lobe epilepsy. *Proceedings of the National Academy of Sciences*, *119*(45), e2213162119. https://doi.org/10.1073/pnas.2213162119

Gy, H., Lj, X., Kl, L., C, Z., Xq, Z., Y, Y., Gm, Z., Yj, W., L, M.-R., Db, M., E, G., C, L., Pd, L., B, C., & Cw, L. (2011). Evaluating the role of connexin43 in congenital heart disease: Screening for mutations in patients with outflow tract anomalies and the analysis of knock-in mouse models. *Journal of Cardiovascular Disease Research*, *2*(4), 206. https://doi.org/10.4103/0975-3583.89804

Hernandez, M. L., Chatlos, T., Gorse, K. M., & Lafrenaye, A. D. (2019). Neuronal Membrane Disruption Occurs Late Following Diffuse Brain Trauma in Rats and Involves a Subpopulation of NeuN Negative Cortical Neurons. *Frontiers in Neurology*, *10*. https://doi.org/10.3389/fneur.2019.01238

Hirschhäuser, C., Lissoni, A., Görge, P. M., Lampe, P. D., Heger, J., Schlüter, K.-D., Leybaert, L., Schulz, R., & Boengler, K. (2021). Connexin 43 phosphorylation by casein kinase 1 is essential for the cardioprotection by ischemic preconditioning. *Basic Research in Cardiology*, *116*(1), 21. https://doi.org/10.1007/s00395-021-00861-z

Ichkova, A., Fukuda, A. M., Nishiyama, N., Paris, G., Obenaus, A., & Badaut, J. (2019). Small Interference RNA Targeting Connexin-43 Improves Motor Function and Limits Astrogliosis After Juvenile Traumatic Brain Injury. *ASN Neuro*, *11*, 1759091419847090. https://doi.org/10.1177/1759091419847090

Johnson, R. G., Le, H. C., Evenson, K., Loberg, S. W., Myslajek, T. M., Prabhu, A., Manley, A.-M., O'Shea, C., Grunenwald, H., Haddican, M., Fitzgerald, P. M., Robinson, T., Cisterna, B. A., Sáez, J. C., Liu, T.-F., Laird, D. W., & Sheridan, J. D. (2016). Connexin Hemichannels: Methods for Dye Uptake and Leakage. *The Journal of Membrane Biology*, *249*(6), 713–741. https://doi.org/10.1007/s00232-016-9925-y

Khan, D., Dupper, A., Deshpande, T., Graan, P. N. E. D., Steinhäuser, C., & Bedner, P. (2016). Experimental febrile seizures impair interastrocytic gap junction coupling in juvenile mice. *Journal of Neuroscience Research*, *94*(9), 804–813. https://doi.org/10.1002/jnr.23726

Lampe, P. D., TenBroek, E. M., Burt, J. M., Kurata, W. E., Johnson, R. G., & Lau, A. F. (2000). Phosphorylation of connexin43 on serine368 by protein kinase C regulates gap junctional communication. *The Journal of Cell Biology*, *149*(7), 1503–1512. https://doi.org/10.1083/jcb.149.7.1503

Mantua, J., Henry, O. S., Garskovas, N. F., & Spencer, R. M. C. (2017). Mild Traumatic Brain Injury Chronically Impairs Sleep- and Wake-Dependent Emotional Processing. *Sleep*, *40*(6), zsx062. https://doi.org/10.1093/sleep/zsx062

Marmarou, A., Abd-Elfattah Foda, M. A., Van den Brink, W., Campbell, J., Kita, H., & Demetriadou, K. (1994). A new model of diffuse brain injury in rats. Part I: Pathophysiology and biomechanics. *Journal of Neurosurgery*, *80*(2), 291–300. https://doi.org/10.3171/jns.1994.80.2.0291

Martins-Marques, T., Catarino, S., Marques, C., Matafome, P., Ribeiro-Rodrigues, T., Baptista, R., Pereira, P., & Girão, H. (2015). Heart ischemia results in connexin43 ubiquitination localized at the intercalated discs. *Biochimie*, *112*, 196–201. https://doi.org/10.1016/j.biochi.2015.02.020

Martins-Marques, T., Ribeiro-Rodrigues, T., Batista-Almeida, D., Aasen, T., Kwak, B. R., & Girao, H. (2019). Biological Functions of Connexin43 Beyond Intercellular Communication. *Trends in Cell Biology*, *29*(10), 835–847. https://doi.org/10.1016/j.tcb.2019.07.001

Masaki, K. (2015). Early disruption of glial communication via connexin gap junction in multiple sclerosis, Baló's disease and neuromyelitis optica. *Neuropathology*, *35*(5), 469–480. https://doi.org/10.1111/neup.12211

Munoz-Ballester, C., Mahmutovic, D., Rafiqzad, Y., Korot, A., & Robel, S. (2022). Mild Traumatic Brain Injury-Induced Disruption of the Blood-Brain Barrier Triggers an Atypical Neuronal Response. *Frontiers in Cellular Neuroscience*, *16*, 821885. https://doi.org/10.3389/fncel.2022.821885

Nichols, J. N., Deshane, A. S., Niedzielko, T. L., Smith, C. D., & Floyd, C. L. (2016). Greater neurobehavioral deficits occur in adult mice after repeated, as compared to single, mild traumatic brain injury (mTBI). *Behavioural Brain Research*, *298*(Pt B), 111–124. https://doi.org/10.1016/j.bbr.2015.10.052

Nielsen, B. S., Hansen, D. B., Ransom, B. R., Nielsen, M. S., & MacAulay, N. (2017). Connexin Hemichannels in Astrocytes: An Assessment of Controversies Regarding Their Functional Characteristics. *Neurochemical Research*, *42*(9), 2537–2550. https://doi.org/10.1007/s11064-017-2243-7 PMID - 28434165

Orellana, J. A., Shoji, K. F., Abudara, V., Ezan, P., Amigou, E., Sáez, P. J., Jiang, J. X., Naus, C. C., Sáez, J. C., & Giaume, C. (2011). Amyloid β-induced death in neurons involves glial and neuronal hemichannels. *The Journal of Neuroscience: The Official Journal of the Society for Neuroscience*, *31*(13), 4962–4977. https://doi.org/10.1523/JNEUROSCI.6417-10.2011

Padget, R. L., Zeitz, M. J., Blair, G. A., Wu, X., North, M. D., Tanenbaum, M. T., Stanley, K. E., Phillips, C. M., King, D. R., Lamouille, S., Gourdie, R. G., Hoeker, G. S., Swanger, S. A., Poelzing, S., & Smyth, J. W. (2024). Acute Adenoviral Infection Elicits an Arrhythmogenic Substrate Prior to Myocarditis. *Circulation Research*, *134*(7), 892–912. https://doi.org/10.1161/CIRCRESAHA.122.322437

Retamal, M. A., Cortés, C. J., Reuss, L., Bennett, M. V. L., & Sáez, J. C. (2006). S-nitrosylation and permeation through connexin 43 hemichannels in astrocytes: Induction by oxidant stress and reversal by reducing agents. *Proceedings of the National Academy of Sciences of the United States of America*, *103*(12), 4475–4480. https://doi.org/10.1073/pnas.0511118103

Rouach, N., Koulakoff, A., Abudara, V., Willecke, K., & Giaume, C. (2008). Astroglial metabolic networks sustain hippocampal synaptic transmission. *Science (New York, N.Y.)*, *322*(5907), 1551–1555. https://doi.org/10.1126/science.1164022

Rovegno, M., Soto, P. A., Sáez, P. J., Naus, C. C., Sáez, J. C., & von Bernhardi, R. (2015). Connexin43 hemichannels mediate secondary cellular damage spread from the trauma zone to distal zones in astrocyte monolayers. *GLIA*, *63*(7), 1185–1199. https://doi.org/10.1002/glia.22808

Sagar, G. D. V., & Larson, D. m. (2006). Carbenoxolone inhibits junctional transfer and upregulates connexin43 expression by a protein kinase A-dependent pathway. *Journal of Cellular Biochemistry*, *98*(6), 1543–1551. https://doi.org/10.1002/jcb.20870

Sarrouilhe, D., Dejean, C., & Mesnil, M. (2017). Connexin43- and Pannexin-Based Channels in Neuroinflammation and Cerebral Neuropathies. *Frontiers in Molecular Neuroscience*, *10*, 320. https://doi.org/10.3389/fnmol.2017.00320

Shandra, O., & Robel, S. (2020). Inducing Post-Traumatic Epilepsy in a Mouse Model of Repetitive Diffuse Traumatic Brain Injury. *J Vis Exp*, *156*. https://doi.org/10.3791/60360

Shandra, O., Winemiller, A. R., Heithoff, B. P., Munoz-Ballester, C., George, K. K., Benko, M. J., Zuidhoek, I. A., Besser, M. N., Curley, D. E., Edwards, G. F., Mey, A., Harrington, A. N., Kitchen, J. P., & Robel, S. (2019). Repetitive Diffuse Mild Traumatic Brain Injury Causes an Atypical Astrocyte Response and Spontaneous Recurrent Seizures. *The Journal of Neuroscience : The Official Journal of the Society for Neuroscience*, *39*(10), 1944–1963. https://doi.org/10.1523/JNEUROSCI.1067-18.2018

Sirnes, S., Kjenseth, A., Leithe, E., & Rivedal, E. (2009). Interplay between PKC and the MAP kinase pathway in Connexin43 phosphorylation and inhibition of gap junction intercellular communication. *Biochemical and Biophysical Research Communications*, *382*(1), 41–45. https://doi.org/10.1016/j.bbrc.2009.02.141

Smyth, J. W., Zhang, S.-S., Sanchez, J. M., Lamouille, S., Vogan, J. M., Hesketh, G. G., Hong, T., Tomaselli, G. F., & Shaw, R. M. (2014). A 14-3-3 mode-1 binding motif initiates gap junction internalization during acute cardiac ischemia. *Traffic (Copenhagen, Denmark)*, *15*(6), 684–699. https://doi.org/10.1111/tra.12169

Sødal, H. F., Nordseth, T., Rasmussen, A. J. O., Rosseland, L. A., Stenehjem, J. S., Gran, J. M., Helseth, E., & Taubøll, E. (2024). Risk of epilepsy after traumatic brain injury: A nationwide Norwegian matched cohort study. *Frontiers in Neurology*, *15*. https://doi.org/10.3389/fneur.2024.1411692

Steinhäuser, C., Grunnet, M., & Carmignoto, G. (2016). Crucial role of astrocytes in temporal lobe epilepsy. *Neuroscience*, *323*, 157–169. https://doi.org/10.1016/j.neuroscience.2014.12.047

Steinhäuser, C., Seifert, G., & Bedner, P. (2012). Astrocyte dysfunction in temporal lobe epilepsy: K+ channels and gap junction coupling. *Glia*, *60*(8), 1192–1202. https://doi.org/10.1002/glia.22313

Stout, C. E., Costantin, J. L., Naus, C. C. G., & Charles, A. C. (2002). Intercellular calcium signaling in astrocytes via ATP release through connexin hemichannels. *The Journal of Biological Chemistry*, *277*(12), 10482–10488. https://doi.org/10.1074/jbc.M109902200

Verellen, R. M., & Cavazos, J. E. (2010). Post-traumatic epilepsy: An overview. *Therapy*, *7*(5), 527. https://doi.org/10.2217/THY.10.57

Vis, J. C., Nicholson, L. F., Faull, R. L., Evans, W. H., Severs, N. J., & Green, C. R. (1998). Connexin expression in Huntington's diseased human brain. *Cell Biology International*, *22*(11–12), 837–847. https://doi.org/10.1006/cbir.1998.0388

Walrave, L., Pierre, A., Albertini, G., Aourz, N., De Bundel, D., Van Eeckhaut, A., Vinken, M., Giaume, C., Leybaert, L., & Smolders, I. (2018). Inhibition of astroglial connexin43 hemichannels with TAT-Gap19 exerts anticonvulsant effects in rodents. *Glia*, *66*(8), 1788–1804. https://doi.org/10.1002/glia.23341

Wang, J., Yang, Z.-Y., Guo, Y.-F., Kuang, J.-Y., Bian, X.-W., & Yu, S.-C. (2018). Targeting different domains of gap junction protein to control malignant glioma. *Neuro-Oncology*, *20*(7), 885–896. https://doi.org/10.1093/neuonc/nox207

Wu, Z., Xu, H., He, Y., Yang, G., Liao, C., Gao, W., Liang, M., & He, X. (2013). Antisense oligodeoxynucleotides targeting connexin43 reduce cerebral astrocytosis and edema in a rat model of traumatic brain injury. *Neurological Research*, *35*(3), 255–262. https://doi.org/10.1179/1743132813Y.0000000165

Xia, J., Tan, Y., Mao, C., Shen, W., & Zhao, Y. (2024). Remazolam affects the phenotype and function of astrocytes to improve traumatic brain injury by regulating the Cx43. *Experimental Gerontology*, *189*, 112404. https://doi.org/10.1016/j.exger.2024.112404

Ye, Z.-C., Wyeth, M. S., Baltan-Tekkok, S., & Ransom, B. R. (2003). Functional hemichannels in astrocytes: A novel mechanism of glutamate release. *The Journal of Neuroscience : The Official Journal of the Society for Neuroscience*, *23*(9), 3588–3596. https://doi.org/11756501

Figure Legends

Figure 1. Mild TBI induces a heterogenous response in Cx43 protein expression. A Representative western blot of cortical brain samples of Sham, 4 hours post-injury and 3 days post-injury mice against Cx43. The membrane was tested against anti-GAPDH as an internal load control. A global increase in Cx43 was found three days post-injury. Representative western blots presented here have been cropped from a membrane with more time points that have not been included in the final manuscript. **B** Normalized quantification of Cx43/GAPDH protein expression (%) demonstrated an increase in Cx43 protein. **C** Representative Cx43 immunohistochemistry images of cortical tissue demonstrating high variability within the same animal. Left: sham, right: 3 dpi. **D** Same image as in **1C** in which each pixel is colored based on their intensity value. **E** Surface plot of the images in figure **1C** in which each pixel color and height indicates the intensity level of said pixel. **F** No differences were detected in mean fluorescence intensity of immunohistochemistry samples. **G** Mice have more variability in Cx43 levels after mild TBI as demonstrated in normalized means of the standard deviation values for the intensity fluorescence of Cx43 immunohistochemistry samples. **H** No differences were detected in kurtosis in the Cx43 fluorescence intensity when assessing normalized means of the kurtosis values for the intensity fluorescence of Cx43 immunohistochemistry samples. In all graphs, each dot represents one mouse.

Figure 2. Cx43 gap junction density and size are unaffected by mild TBI while soluble Cx43 increases. **A** Representative western blot of solubility-fractionated cortical brain tissue. Sol: soluble fraction, Insol: insoluble fraction. **B** No differences were detected in insoluble Cx43 between sham and 3 dpi animals in the normalized quantification of the insoluble fraction of Cx43 by western blot (%). **C** Cx43 soluble fraction increases after mild TBI. Each dot represents one mouse. P-value of the analysis in the graph. **D** Graph representing the increased ratio of

soluble to insoluble Cx43. **E** Representative immunohistochemistry super-resolution images of Cx43 plaques, in which no changes in density or size were observed. White square indicates area zoomed and their location in the global image. **F** No differences in Cx43 plaque size between sham and 3 dpi mice were detected. In quantification of Cx43 plaque size in sham and 3 dpi. **G** No differences in Cx43 plaque density were detected after TBI in quantification of Cx43 plaque density (plaque/μm^2) in sham and 3 dpi **H** Graph of the cumulative distribution of Cx43 plaque size in μm^2, black line = sham and grey line = 3 dpi. In all bar graphs, each dot represents one mouse.

Figure 3. Mild TBI induces an increase in Cx43 hemichannel-dependent activity. A Representative confocal image of sham and 3 dpi animals. EtBr in magenta and s100b (astrocyte marker) in green. Upper panels: EtBr signal alone. Lower panels: merge imaged of EtBr and s100b. White squares indicate the zoomed area. EtBr fluorescence intensity is increased in astrocytes after mild TBI. **B** Quantification of EtBr fluorescence intensity levels (%) in sham and 3 dpi mice. EtBr fluorescence intensity is increased in 3 dpi mice compared to sham mice. **C** Representative zoomed confocal images of control and CBX-treated astrocyte of a 3 dpi mouse. Green: s100b, magenta: EtBr. **D** Quantification of EtBr fluorescence intensity levels in control and CBX-treated slices of 3 dpi mice. EtBr fluorescence intensity is decreased in CBX-treated slices compared to control. **E** Representative zoomed confocal images of a control and a TAT-Gap19-treated astrocyte of a 3 dpi mouse. Green: s100b, magenta: EtBr. **F** Quantification of EtBr fluorescence intensity levels (%) in control and TAT-Gap19-treated slices of 3 dpi mice. Red dots and lines indicate the samples that do not follow the pattern of decrease in fluorescence intensity. EtBr fluorescence intensity is decreased in TAT-Gap19-treated slices compared to control. In all graphs, each dot represents one mouse.

Figure 4. Phosphorylation of Cx43^{S368} after mild TBI increases seizure susceptibility. A Representative western blot of cortical brain samples of Sham and 3 dpi mice against pCx43^{S368} and Cx43 proteins. As an internal loading control, the membranes were tested against GAPDH. After mild TBI, pCx43^{S368} is increased. Two independent gels with the same samples were run. Representative western blots presented here have been cropped from a membrane with more time points that have not been included in the final manuscript. **B** Normalized quantification of the percentage of Cx43 which has been phosphorylated at the serine 368 residue (pCx43^{S368}) from western blots in A. Data are presented as a ratio between pCx43^{S368} normalized to GAPDH and Cx43 normalized to GAPDH (%). pCx43^{S368} is significantly increased after mild TBI. **C** Western blot of cortical brain samples of C57Bl/6 and Cx43^{S368A} mice against pCx43^{368} and Cx43 proteins. As an internal loading control, the membranes were probed for total protein. The representative total protein membranes presented here are cropped. **D** Normalized quantification of the percentage of Cx43 with pCx43^{S368} from western blots in C. Data are presented as a ratio between pCx43^{S368} normalized to total protein and Cx43 normalized to total protein. The proportion of pCx43 ^{S368} is significantly reduced in Cx43^{S368A} animals. **E** Graph representing the cumulative percentage of naïve C57Bl/6 (dotted green line) and Cx43^{S368A} (dotted purple line) which experienced a tonic-clonic seizure at every PTZ injection number. C57Bl/6 n = 14, Cx43^{S368A} n = 13. Naïve Cx43^{S368A} animals require more PTZ injections to develop tonic-clonic seizures, suggesting their susceptibility to seizures is decreased. **F** Graph representing the cumulative percentage of naïve Sham C57Bl/6 (dark green line), 3 dpi C57Bl/6 (light green light), Cx43^{S368A} sham (dark purple line), Cx43^{S368A} and 3 dpi Cx43^{S368A} (light purple line) which experienced a tonic-clonic seizure at every PTZ injection number. **G** Graph representing the average Racine scale value of each experimental group at every injection number. Sham C57Bl/6 (dark green line), C57Bl/6 (light green line), Cx43^{S368A} sham (dark purple line), Cx43^{S368A} 3 dpi (light purple line). **H** Quantification of the area under the curve of the graph in G. In all bar graphs, each dot represents one mouse.

Figure 5. Gap junction plaque density is reduced in Cx43^{S368A} mice. A Representative immunohistochemistry super-resolution images of Cx43 plaques in C57Bl/6 sham, C57Bl/6 3 dpi, Cx43^{S368A} sham and Cx43^{S368A} 3 dpi mice. Mild TBI does not change Cx43 gap junction plaque size or density but prevention of Cx43^{S368} phosphorylation causes a significant reduction in Cx43 gap junction plaque density in cortex. **B** Quantification of Cx43 plaque size in C57Bl/6 sham, C57Bl/6 3 dpi, Cx43^{S368A} sham and Cx43^{S368A} 3 dpi mice. Mild TBI does not alter Cx43 gap junction plaque size and there is no difference in size between C57Bl/L6 and Cx43^{S368A} mice. **C** Quantification of Cx43 plaque density (plaque/μm^2) in C57Bl/6 sham, C57Bl/6 3 dpi, Cx43^{S368A} sham and Cx43^{S368A} 3 dpi mice. Mild TBI does not change Cx43 plaque density but preventing Cx43^{S368} phosphorylation causes a significant reduction in Cx43 plaque density. In all graphs, each dot represents one mouse.

Table legends

Table 1. Manufacturer information, working dilutions and resource identification numbers for primary and secondary antibodies that were used for western blot.

Table 2. Manufacturer information, working dilutions and resource identification numbers for primary and secondary antibodies that were used for immunohistochemistry.

Supplementary figures and table legends.

Supplementary Figure 1. The pannexin1-blocker spironolactone does not inhibit ethidium bromide uptake in astrocytes after mild TBI. A Representative confocal image of control and spironolactone-treated astrocyte of a 3 dpi mouse. Green: s100b, magenta: EtBr. **B** Quantification of EtBr fluorescence intensity levels in control and spironolactone-treated slices of 3 dpi mice. Each dot represents one mouse. EtBr fluorescence intensity does not change in spironolactone-treated slices compared to control.

Supplementary figure 2. Cx43 and panCx43 stainings indicate the same changes in Cx43 density between C57Bl/6 and S368A animals. A Representative immunohistochemistry super-resolution images of Cx43 and panCx43 plaques in C57Bl/6 sham, C57Bl/6 3 dpi, $Cx43^{S368A}$ sham and $Cx43^{S368A}$ 3 dpi mice. Differences in image intensity, plaque density, and plaque size between the groups are the same for Cx43 and panCx43 IHC. **B** Quantification of image intensity in C57Bl/6 sham, C57Bl/6 3 dpi, $Cx43^{S368A}$ sham and $Cx43^{S368A}$ 3 dpi mice. **C** Quantification of plaque density normalized to C57Bl/6 sham in C57Bl/6 sham, C57Bl/6 3 dpi, $Cx43^{S368A}$ sham and $Cx43^{S368A}$ 3 dpi mice. **D** Quantification of plaque size normalized to C57Bl/6 sham in C57Bl/6 sham, C57Bl/6 3 dpi, $Cx43^{S368A}$ sham and $Cx43^{S368A}$ 3 dpi mice. In all graphs, each dot represents one mouse.

Supplementary table 1. Table with all results for PTZ experiments per animal.

Figure 1

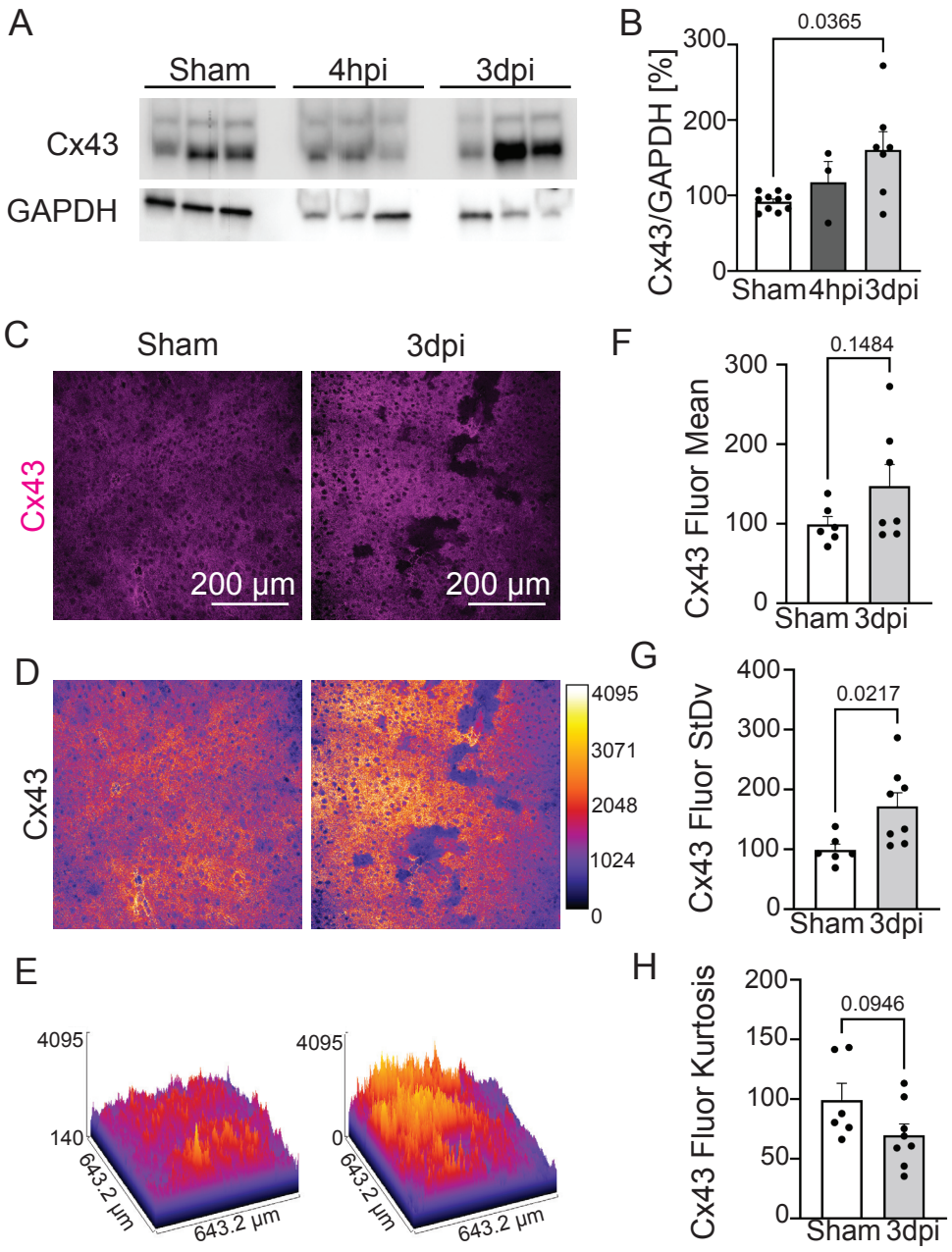

Figure 2

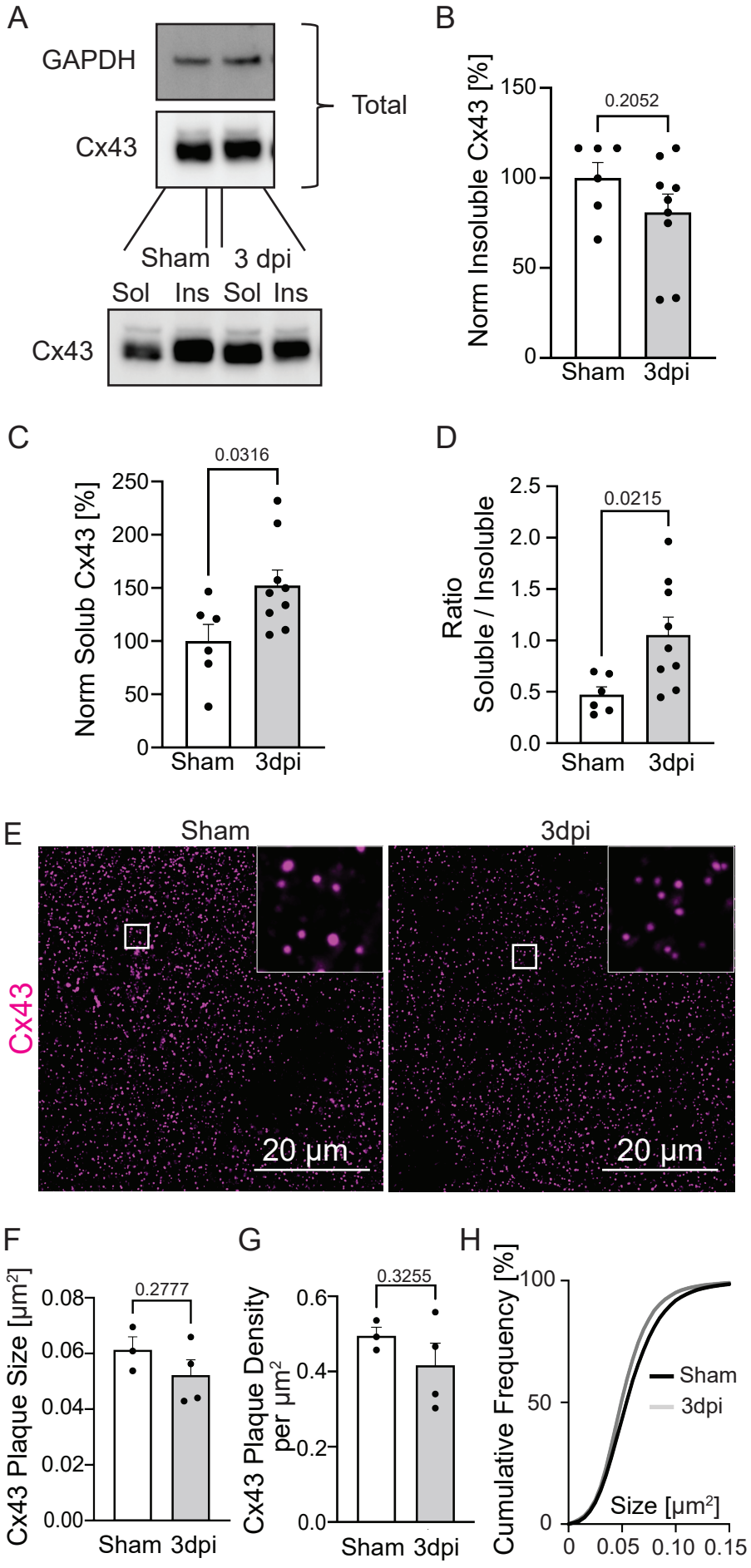

Figure 3

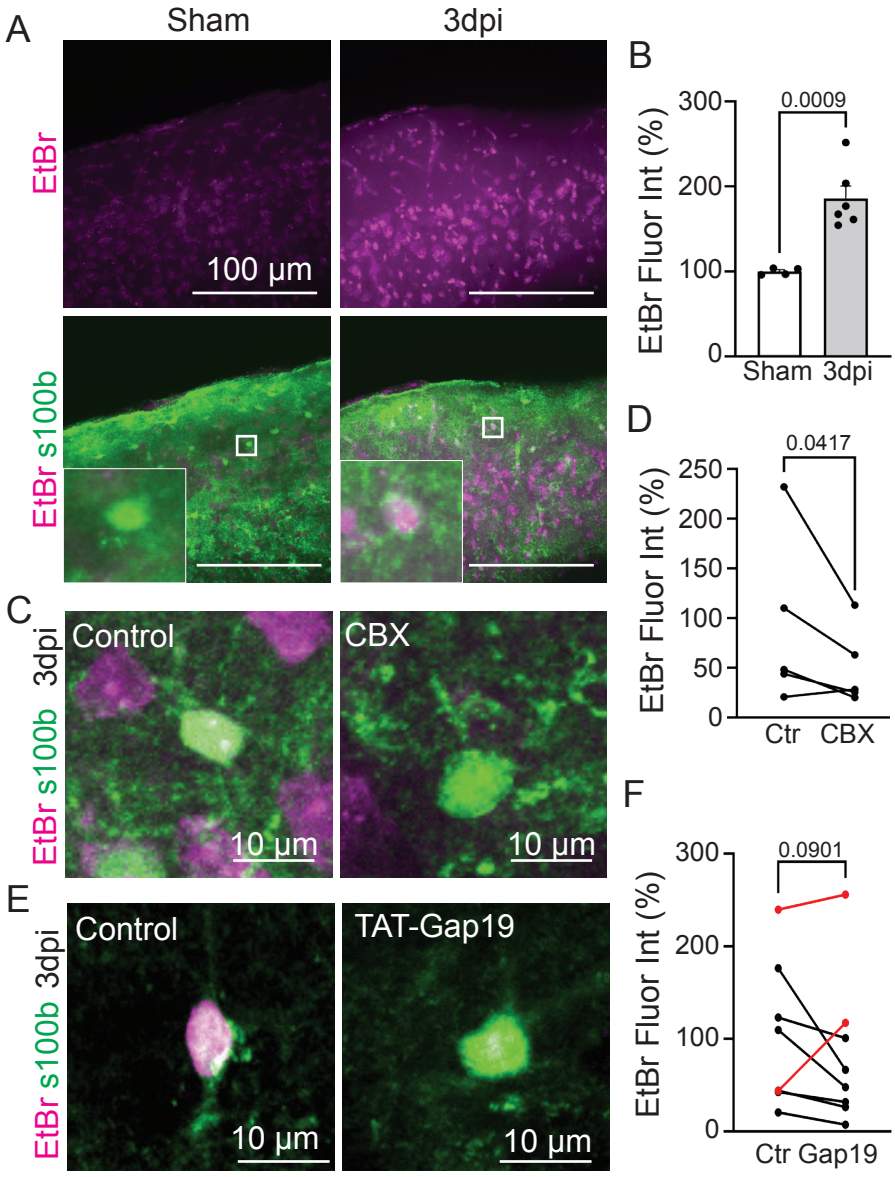

Figure 4

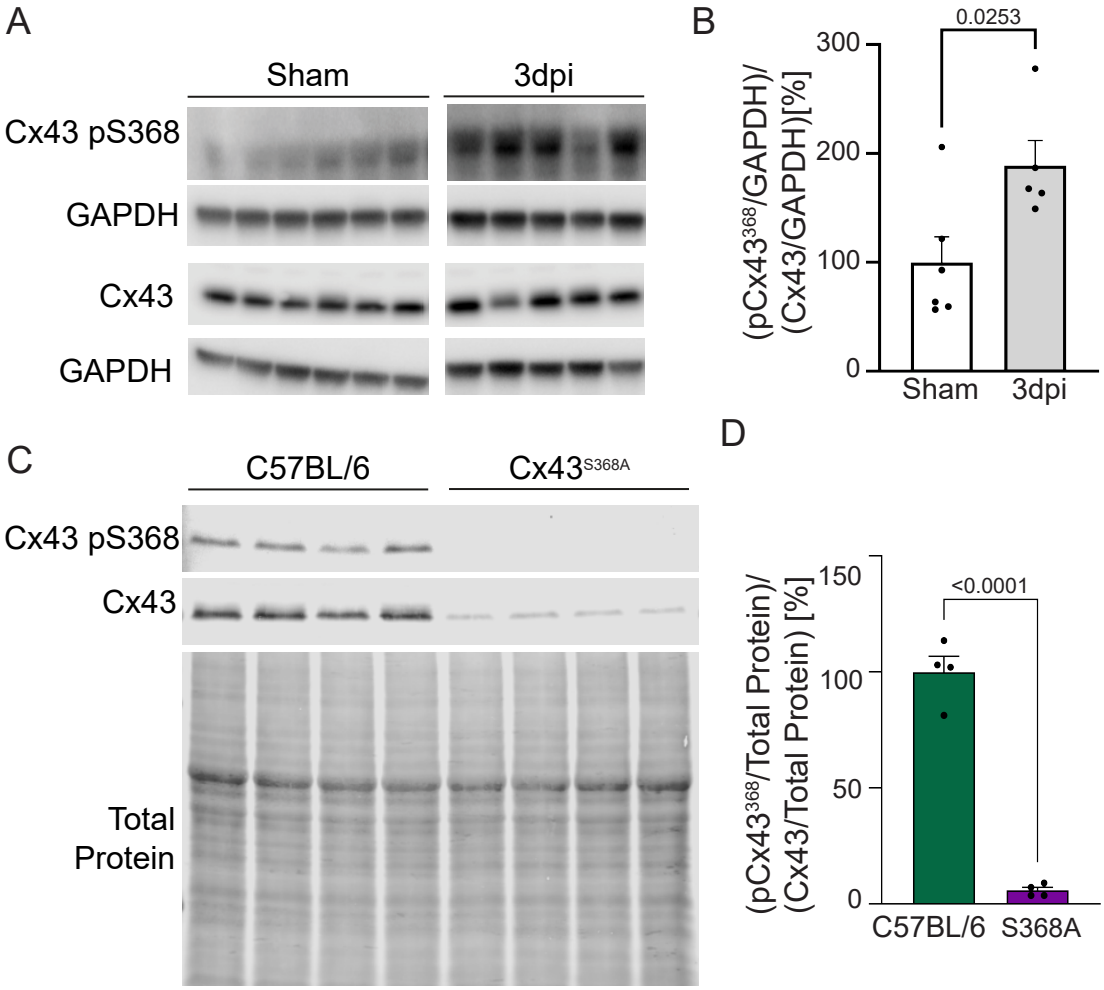

Figure 5

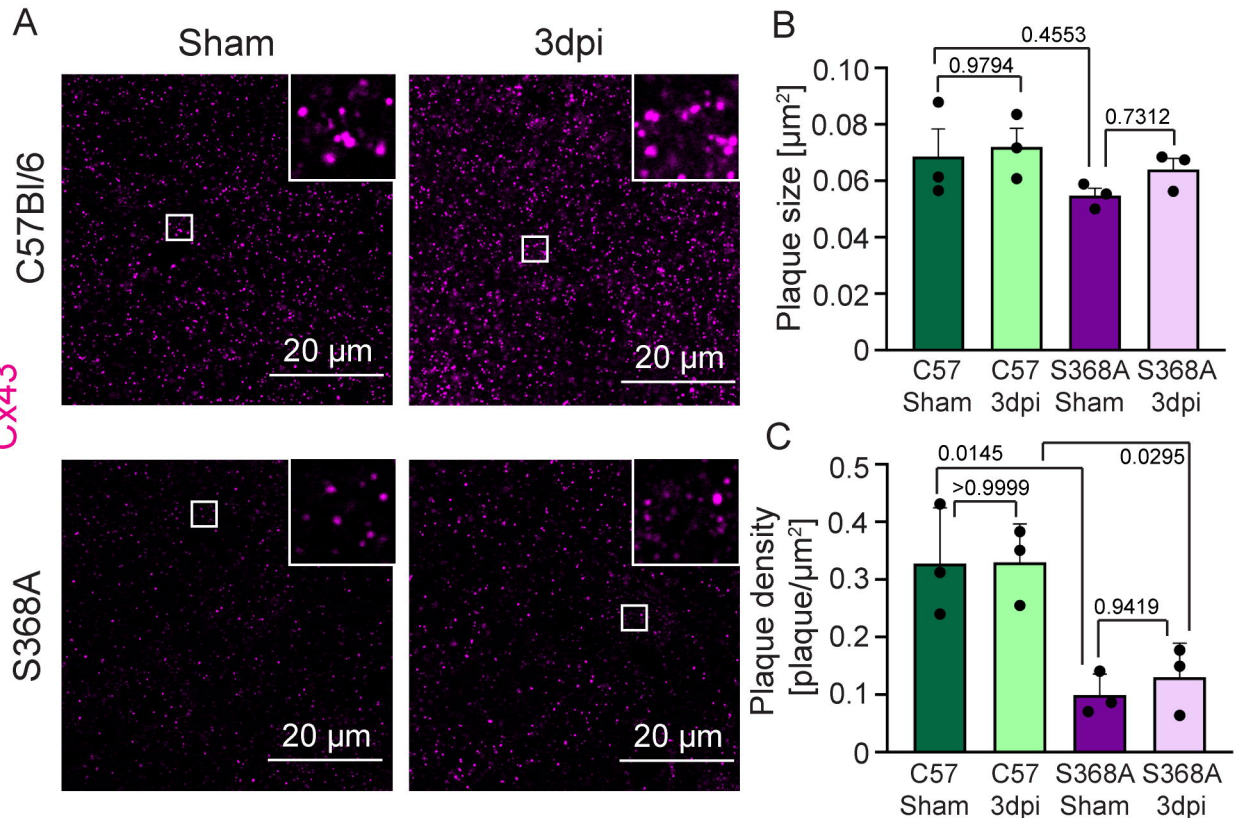
A
Sham
3dpi
C57Bl/6
S368A
Cx43
20 µm
20 µm
20 µm
20 µm
B
Plaque size [µm²]
0.10
0.08
0.06
0.04
0.02
0
0.9794
0.4553
0.7312
C57 Sham
C57 3dpi
S368A Sham
S368A 3dpi
C
Plaque density [plaque/µm²]
0.5
0.4
0.3
0.2
0.1
0
0.0145
>0.9999
0.0295
0.9419
C57 Sham
C57 3dpi
S368A Sham
S368A 3dpi

Table 1

Manufacturer information, working dilutions and resource identification numbers for primary and secondary antibodies that were used for western blot.

Target protein	Manufacturer	Catalog #	RRID	Species Raised In	Monoclonal / Polyclonal	Concentration	Figure in which it was used
Primary Antibodies							
Cx43	Sigma-Aldrich	C6219	AB_476857	Rabbit	Polyclonal	1:3000	Fig. 1A, Fig. 2A, Fig. 4A
Cx43	Millipore	MAB3067	AB_94663	Mouse	Monoclonal	1:1000	Fig. 4C
pCx43S368	Thermo Fisher Scientific	48-3000	AB_2533845	Rabbit	Polyclonal	1:1000	Fig. 4A, Fig. 4C
GAPDH	Abcam	ab8245	AB_2107448	Mouse	Monoclonal	1:5000	Fig. 1A, Fig. 2A, Fig. 4A
Secondary Antibodies							
Rabbit IgG HRP	Santa Cruz Biotechnology	sc-2357	AB_628497	Mouse	Monoclonal	1:5000	Fig. 1A, Fig. 2A, Fig. 4A
m-IgGκ BP-HRP	Santa Cruz Biotechnology	sc-516102	AB_2687626		Monoclonal	1:5000	Fig. 1A, Fig. 2A, Fig. 4A
Rabbit IgG IR700	AzureSpectra	AC2128	AB_3665331	Goat	Unknown	1:5000	Fig. 4C
Mouse IgG IR800	AzureSpectra	AC2135	AB_3665332	Goat	Unknown	1:5000	Fig. 4C

Table 2

Manufacturer information, working dilutions and resource identification numbers for primary and secondary antibodies that were used for immunohistochemistry.

Target protein	Manufacturer	Catalog #	RRID	Species Raised In	Monoclonal/ Polyclonal	Concentration	Figure in which it was used
Primary Antibodies							
Cx43	Sigma-Aldrich	C6219	AB_476857	Rabbit	Polyclonal	1:1000	Fig. 1C, D; Fig. 2E; Fig. 5A; Suppl Fig. 1
Cx43	Abcam	ab87645	AB_1951148	Goat	Polyclonal	1:250	Suppl Fig. 1
S100β	Sigma-Aldrich	S2532	AB_477499	Mouse	Monoclonal	1:1000	Fig. 3
Secondary Antibodies							
Rabbit Alexa-488	Jackson Immuno Research	111-546-144	AB_2338057	Goat	Polyclonal	1:1000	Fig. 1C, D; Fig. 2E; Fig. 5A; Suppl Fig. 1
Mouse Alexa-647	Jackson Immuno Research	115-606-003	AB_2338921	Goat	Polyclonal	1:1000	Fig. 3
Goat Alexa-488	Jackson Immuno Research	705-545-003	AB_2340428	Goat	Polyclonal	1:1000	Suppl Fig. 1